



Structural Elucidation and Magnetic Behavior Evaluation of Nd-doped Nickel-Cobalt Spinel Ferrites

Muhammad Waqar¹, A. I. Aljameel^{2*}

¹ Institute of Physics, The Islamia University of Bahawalpur, Bahawalpur-63100, Pakistan

² Department of Physics, College of Science, Imam Mohammad Ibn Saud Islamic University (IMSIU), Riyadh 11623, Saudi Arabia

ARTICLE INFO

Article History:

Received: April 08, 2021

Revised: May 14, 2021

Accepted: June 28, 2021

Available Online: June 30, 2021

Keywords:

XRD

FTIR

Magnetic Properties

Coercivity

Remanence Ratio

ABSTRACT

Nano ferrites crystals of $Ni_{0.4}Co_{0.6}Nd_xFe_{2-x}O_4$ for $0.00 \leq x \leq 0.08$ with step size of 0.02 were synthesized by sol gel technique with annealing at 950 °C for 6 hours. Spinel phase along with a secondary phase for Nd concentration $x \geq 0.04$ due to formation of $NdFeO_3$ was observed in XRD patterns. Lattice constant and grain size were found in decreasing trend with increasing concentration of Nd as compared to that of undoped nickel cobalt ferrites. X-ray density and porosity both were increased with increasing concentration of neodymium. Two characteristics frequency bands were observed in the range of 400cm^{-1} to 550cm^{-1} which showed successful formation of spinel structure. It is also the evidence of metal-oxygen bonding at octahedral and tetrahedral sites in spinel ferrites. Also, bands for carbon-hydrogen, carboxyl group, carbon-oxygen stretching and iron-cobalt alloys were observed in the FTIR spectra. By using these values of characteristics frequencies, octahedral and tetrahedral radii were calculated and found in decreasing trend with increasing concentration. Force constants are increasing with increase in neodymium concentration. Saturation magnetization, coercivity and remanence values were calculated from the M-H loops. Saturation magnetization showed the decreasing behavior with increase in neodymium concentration. Coercivity showed increasing values as compared to the base sample and also showing reciprocal relation with saturation magnetization. Magnetic moment is decreasing with increase in neodymium concentration.

OPEN ACCESS

© 2021 The Authors, Published by iRASD. This is an Open Access article under the Creative Common Attribution Non-Commercial 4.0

*Corresponding Author's Email: jameel@imau.edu.sa

1. Introduction

In today's world we are surrounded by magnetic materials which occurs naturally as well as in many technologies. They have a variety of applications which encompass vast range of fields from computer technology, audio, video applications, telecommunication technology, transportation and energy supply. Automotive industry uses them in their sensory applications and electric motors, medical imaging and stealthy aircrafts also make use of magnetic materials.

Over the years, the production, characterization and application of nanoparticles have gained prominence due to the immense potential present in its application in the environmental, electronics and biomedical fields. In this context, the special properties related to manufacturing processes make nanoparticles a fertile field for technological applications. Many researchers have studied different properties of spinel ferrites due to their importance in a wide variety of fields (Pardavi-Horvath, 2000).

The influence of neodymium (Nd) substitution on the dielectric, electrical and structural properties of Nickel cobalt crystals with composition $\text{Ni}_x\text{Co}_{1-x}\text{Nd}_y\text{Fe}_{2-y}\text{O}_4$ ($0.00 \leq x \leq 1.00$ and $0.00 \leq y \leq 0.10$) was studied by M. T. Farid et. al using sol gel method. Secondary phase of iron neodymium oxide (NdFeO_3) was also observed along with the spinel phase when $y \geq 0.06$. Due to greater ionic radius of neodymium as compared to Iron, a trivial increase in lattice parameter was also detected and Neodymium substitution restricted the grain growth. It was observed that DC resistivity increased with the increase in neodymium concentration. Also rise in temperature led to drop in DC resistivity thus proving the semiconducting materials. The AC-conductivity, dielectric loss ($\tan \delta$) and dielectric constant were reduced because of neodymium doping. Due to smaller values of conductivity at room temperature these prepared compositions can be used for the microwave applications that need insignificant eddy currents. The reduction in dielectric constant is attributed to the decrease in the internal viscosity of the samples and this can be explained based on space charge polarization. (M. Farid et al., 2015).

In another paper M. T Farid et. al discuss the structure, dielectric and electric properties of different composition by using the sol gel technique. X-ray diffraction analysis revealed that $\text{Ni}_x\text{Co}_{1-x}\text{Pr}_y\text{Fe}_{2-y}\text{O}_4$ ($0.00 \leq x \leq 1.00$ and $0.00 \leq y \leq 0.10$) samples clearly indicate formation of cubic spinel crystals. In the last three samples secondary phase was also identified. Lattice constant exhibited increase from 8.363 \AA to 8.384 \AA with rising Pr concentration. DC resistivity at room temperature of ferrites $\text{Ni}_x\text{Co}_{1-x}\text{Pr}_y\text{Fe}_{2-y}\text{O}_4$ was increased with increase in praseodymium concentration. The introduction of Pr^{3+} replacement with Fe^{3+} caused a minor rise in lattice parameter because of greater ionic radius of the doping ions. The grain growth was hindered by doping of praseodymium. Temperature dependent direct current electrical resistivity was observed to decrease as the temperature increased which indicated semi-conductor behavior of the samples. These prepared compositions can also be utilized in microwave communication due to low values of dielectric loss and dielectric constant. This synthesized ferrite may be appropriate for applications in the high frequency ranges as having lower values of eddy current losses by the consequence of high DC resistivity values. Calculated drift mobility increased with increase in temperature. The dielectric constant value for $y = 0.00$ were very greater as compared to $y = 0.10$. In accordance with previous studies, it was observed that the AC-conductivity, dielectric loss ($\tan \delta$) and dielectric constant reduced because of Pr^{3+} substitution (M. T. Farid, Ahmad, Murtaza, Ali, & Ahmad, 2016).

Rare earth La^{3+} material substituted in Nickel-Cobalt nanocrystalline ferrites were synthesized by sol gel technique. $\text{Ni}_{0.5}\text{Co}_{0.5}\text{La}_x\text{Fe}_{2-x}\text{O}_4$ (where $x = 0.025, 0.050, 0.075, 0.100$ and 0.125) nanoparticles was carried out at different percentage of La^{3+} compositions with analytical grade metal nitrate. The fabricated samples have sintered at 400°C and characterized by XRD. Scherrer's formula was used to calculate the particle size. The nanoparticles dimensions of $\text{NiCoFe}_2\text{O}_4$ with the influence of La^{3+} was investigated in the range of 23.30 to 32.31 nm range. The crystallite size was observed to be constant with increasing of the Lanthanum contains in the compositions. Also, the magnetic properties of prepared samples were studied by Hysteresis loop terser. We have successfully Synthesized Nanoparticles of $\text{Ni}_{0.5}\text{Co}_{0.5}\text{La}_x\text{Fe}_{2-x}\text{O}_4$. The XRD pattern of synthesized samples confirmed phase formation of $\text{Ni}_{0.5}\text{Co}_{0.5}\text{La}_x\text{Fe}_{2-x}\text{O}_4$ ferrite. The particle size calculated from X-ray diffraction it showed constant in particle size. From the Magnetic properties, it was cleared that the prepared material was soft ferrite. The magnetic saturation changed with substitution of different compositions (KULKARNI, BHUJBAL, & RATHOD, 2016).

2. Materials and Methods

More than a few approaches have been testified to produce nanocrystalline spinel ferrites; these include Powder Ceramic technique (Kriebler, Lo, Melikhov, & Snyder, 2006), Micro-emulsion method (Iqbal & Siddiquah, 2008), Chemical Coprecipitation method (Anis-ur-Rehman, Ansari, Mughal, Awan, & Maqsood, 2012) and Soft Citrate-gel method (Hankare, Sankpal, Patil, Lokhande, & Sasikala, 2011).

In the current work, sol gel method is used for the preparation of Nd doped nickel cobalt nano crystals. The preference to this method was given as it is a simple, speedy and time saving with less energy feeding as compared to other methods. The

impartial of the current work is to prepare Nd replaced nickel-cobalt nanocrystal using sol gel technique for exploring the magnetic and structural behavior. Nano ferrite of the composition $\text{Ni}_{0.4}\text{Co}_{0.6}\text{Nd}_x\text{Fe}_{2-x}\text{O}_4$ (for $0.00 \leq x \leq 0.08$) has been prepared at a small temperature (90°C) by Citrate-gel auto combustion method.

Nd doped Ni-Co Nano ferrite with the chemical formula $\text{Ni}_{0.4}\text{Co}_{0.6}\text{Nd}_x\text{Fe}_{2-x}\text{O}_4$ (where $0.00 \leq x \leq 0.08$) were synthesized by sol gel technique by using the following starting materials (Cannas, Falqui, Musinu, Peddis, & Piccaluga, 2006). Nickel nitrate, Cobalt acetate, Neodymium trinitrate hexahydrate, Ferric nitrate, Citric Acid and Ammonia and their detailed description of these starting materials required for the synthesis of neodymium doped nickel cobalt nano-ferrites by Sol-gel auto-combustion method. Proper quantities of Nitrates of metals designated in the starting materials for Nd doped Ni-Co nanocrystal system Neodymium Trinitrate, Ferric Nitrate and Nickel Nitrate along with other salts Cobalt acetate and citric acid have been solved in isolated beakers.

The mixture of nitrate was added with the properly calculated quantity of citric acid for the purpose of chelating agent. Magnetic stirrer was used for mixing to get the homogenous solution. Firstly, the solution temperature raised to 90°C then Ammonia solution was added at very slow rate to the Citrate - Nitrate mixture for adjusting the pH in range 7 to 8 for each sample marked number 1 to 5. The mixture solution was maintained about 90°C by continuous stirring with the help of hot magnetic plate for evaporation until a highly sticky gel obtained. Finally, the viscous gel began bubbling and just after it gel started its combustion automatically.

The ashes collected from beakers of each sample were grinded and collected it in the powdered form. Finally, the dried and grinded sample of each composition of $\text{Ni}_{0.4}\text{Co}_{0.6}\text{Nd}_x\text{Fe}_{2-x}\text{O}_4$ ferrite was annealed by using the controlled Muffle Furnace Vulcan A-550 as shown in figure. The annealing was done for 6 hours continuously and the temperature of the annealing was kept at 950°C to obtain the proper spinel phase. After this all samples were ed into fine powder. Several methods were used to find the different characteristics of the prepared samples with different compositions for analysis and investigation which are: XRD, FTIR, VSM.

3. Results and Discussion

3.1. Structural Analysis

The nanocrystals of $\text{Ni}_{0.4}\text{Co}_{0.6}\text{Nd}_x\text{Fe}_{2-x}\text{O}_4$ spinel ferrites with $0.00 \leq x \leq 0.08$ were synthesized by sol gel technique. The structural elucidation and magnetic behavior of Nd doped Ni-Co ferrite studied with changed concentrations of neodymium in Ni-Co spinel ferrite. With the help of these observations, the substitution and distribution of Nd^{3+} in A and B sublattices of nickel-cobalt ferrites was studied. The XRD peaks of neodymium doped nickel-cobalt nanocrystals with step size $x = 0.00, 0.02, 0.04, 0.06$ and 0.08 are shown in figure1 for all the prepared samples.

Table 1
X-ray density, Secondary phase, porosity, lattice parameter and grain size of $\text{Ni}_{0.4}\text{Co}_{0.6}\text{Nd}_x\text{Fe}_{2-x}\text{O}_4$ for $0.00 \leq x \leq 0.08$

Sample Compositions	Secondary Phase	Lattice Constant a (Å)	X-ray Density (g/cm^3)	Grain Size (nm)	Porosity
$\text{Ni}_{0.4}\text{Co}_{0.6}\text{Fe}_2\text{O}_4$	---	8.373033	5.309609	25.90719	0.328702
$\text{Ni}_{0.4}\text{Co}_{0.6}\text{Nd}_{0.02}\text{Fe}_{1.98}\text{O}_4$	---	8.366359	5.362448	23.23839	0.426503
$\text{Ni}_{0.4}\text{Co}_{0.6}\text{Nd}_{0.04}\text{Fe}_{1.96}\text{O}_4$	NdFeO ₃	8.35285	5.428825	22.98876	0.60207
$\text{Ni}_{0.4}\text{Co}_{0.6}\text{Nd}_{0.06}\text{Fe}_{1.94}\text{O}_4$	NdFeO ₃	8.366754	5.441921	23.90425	0.426871
$\text{Ni}_{0.4}\text{Co}_{0.6}\text{Nd}_{0.08}\text{Fe}_{1.92}\text{O}_4$	NdFeO ₃	8.355141	5.504928	23.97696	0.480963

The comparison of these peaks patterns for each sample with the reference data from the ICDD Nos. CoFe_2O_4 (00-01-1121) and NiFe_2O_4 (00-03-0875) revealed the crystalline phases. The observed patterns showed a cubic spinel structure of single phase with another peak for secondary phase at $x \geq 0.04$. The observed Bragg's reflections were indexed as (220), (311), (222), (400), (422), (511) and (440) with 2θ ranging from 25 to

80 degrees. X-ray density, Secondary phase, grain size and lattice parameter (a) are recorded for $\text{Ni}_{0.4}\text{Co}_{0.6}\text{Nd}_x\text{Fe}_{2-x}\text{O}_4$ ferrites system along with the compositions in following Table1.

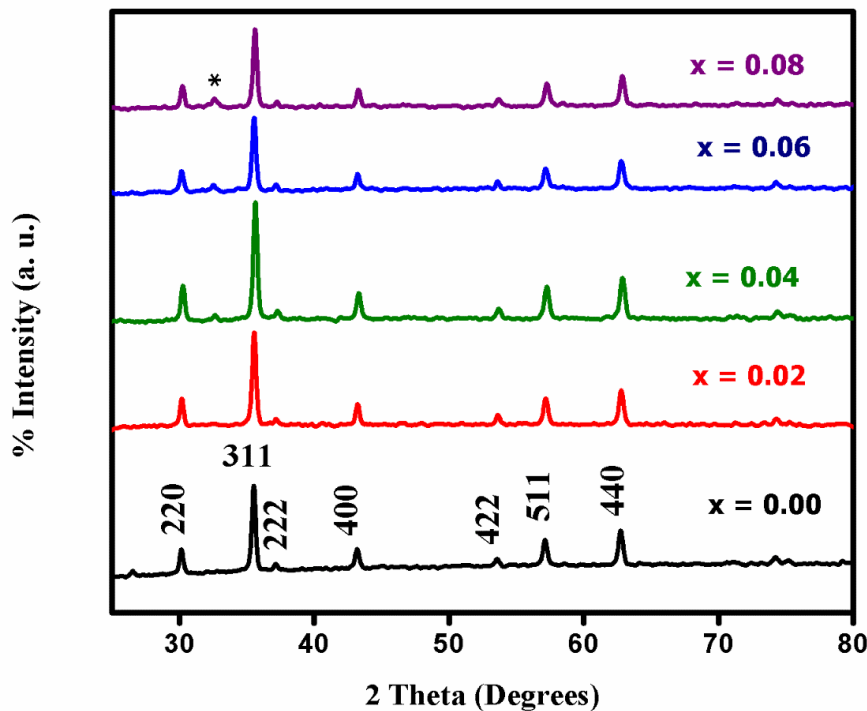


Figure 1: XRD patterns of $\text{Ni}_{0.4}\text{Co}_{0.6}\text{Nd}_x\text{Fe}_{2-x}\text{O}_4$ spinel ferrites with $0.00 \leq x \leq 0.08$

A peak corresponding to $2\theta = 32.6^\circ$ (indicated by * in Fig.1) is denoted as secondary phase for $x \geq 0.04$ at grain boundaries and with increasing concentration of Nd, the intensity of the peak was also increased. The labelled peak recognized as NdFeO_3 (Iron Neodymium Oxide) corresponding with ICDD No. 74-2203. This appearance of secondary phase is the consequence of larger reactivity of Fe^{3+} with the neodymium Nd^{3+} . It also confirms that Nd^{3+} ion replacement has the solubility bound in lattice of Nd doped nickel cobalt ferrites. The lattice parameter and distance between adjacent Miller planes (h, k, l) were determined according to Bragg's equation for cubic lattice as:

$$a = \lambda \frac{(h^2 + k^2 + l^2)^{\frac{1}{2}}}{2 \sin \theta} \quad (1)$$

Where a is lattice parameter, (h, k, l) are the interplanar distance, the X-ray wavelength is λ (Anupama & Rudraswamy, 2016). The average particle size estimated from the maximum intensity recorded (311) peaks of X-ray diffraction patterns with the formula given by Scherrer's as:

$$D = \frac{0.9\lambda}{\beta \cos \theta} \quad (2)$$

Where average crystalline size is D of nanocrystal in nano meter, the X-ray wavelength taken 1.54 \AA is denoted by λ , the Bragg's angle is θ and the full width at half maximum (FWHM) is denoted by β . The table1 showed the values of crystallite size and lattice parameter. The calculated values for X-ray density of each sample are tabulated in table1. These values were calculated using the mathematical formula:

$$\rho_x = \frac{8M}{N_A \times V} \quad (3)$$

Where molecular weight is denoted by M of the sample, N_A denotes the Avogadro's number and volume of the cubical unit cell is V .

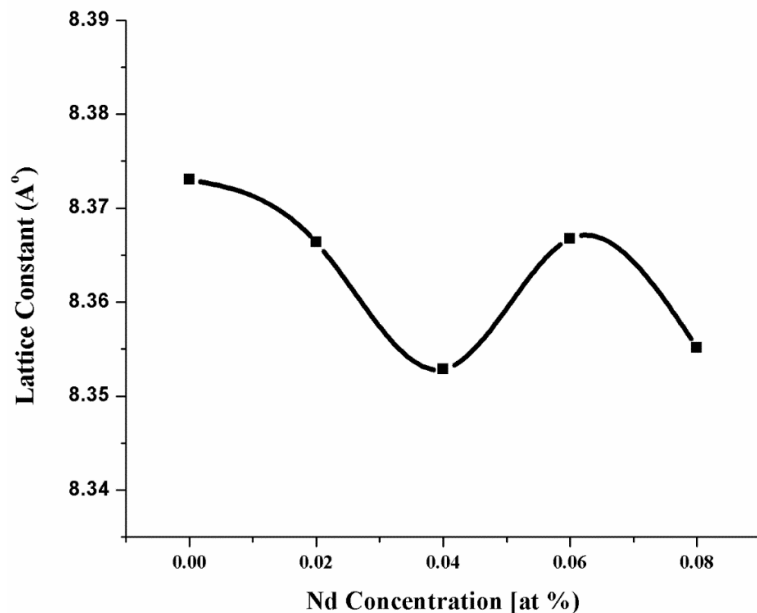


Figure 2: Nd Contents vs Lattice Parameter

The trivial variations are there in lattice parameter 'a' that could be linked in the increasing Nd^{3+} concentration, the ionic radii of Nd^{3+} (0.983 Å) is larger as compared to Fe^{3+} (0.645 Å). The lattice constant first somewhat reduced with neodymium count in the lattice and then increased with higher substitutions and then decreased again, as shown in the Figure 2 and Table 1. It is clearly recognized that the lattice constant is powerfully reliant on the Nd^{3+} ion radii. The substitution of a specific amount of Nd^{3+} ions at the octahedral sites would rise the value of a compared to the undoped $\text{NiCoFe}_2\text{O}_4$ ferrite. The decrease in a by increase in Nd^{3+} amount could be attributed to the ionic rearrangement between the existing interstitial octahedral B and tetrahedral A sites for the spinel frame. Another reasonable description for the experimental reduction in lattice parameter can be made from likely vacancies of iron in the in crystallization process in samples because of the adding of a greater ion size in the B site. In addition that, By increasing of Nd^{3+} concentration, the reduction in lattice parameter could be ascribed to the firmness of spinel lattice made by the secondary phases due to the difference in thermal expansion coefficients (Dasan, Guan, Zahari, & Chuan, 2017).

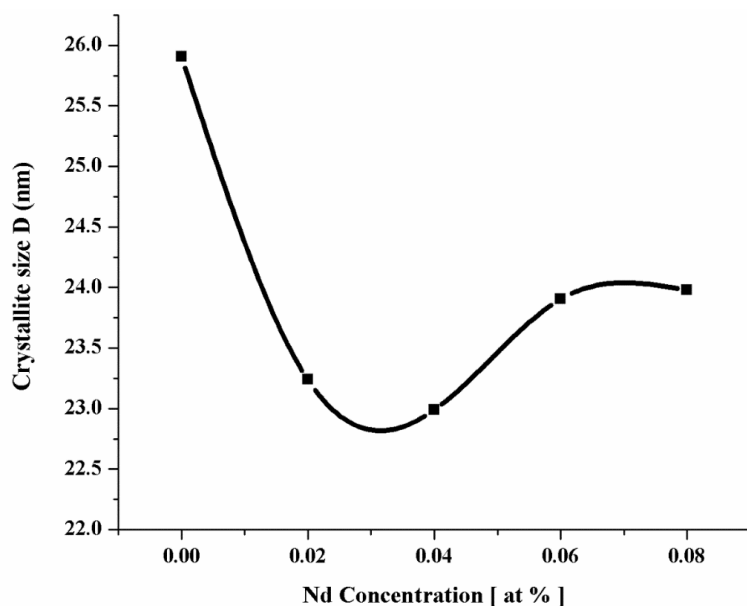


Figure 3: Crystallite size as a function of Nd concentration

Another experimental effect of Neodymium exchange is the drop in the samples' crystallite size. With the addition of Nd amounts, the grain size was showing the reducing trend. The bond energy of $\text{Nd}^{3+}-\text{O}^{2-}$ is higher than that of $\text{Fe}^{3+}-\text{O}^{2-}$ may suggests that additional energy is desired to push the Nd^{3+} to arrive the lattices and $\text{Nd}^{3+}-\text{O}^{2-}$ form

bonding. Consequently, higher thermal stability of the Nd^{3+} substituted ferrites was observed as compared to the pure nickel cobalt ferrites, and higher amount of energy is required for the replaced samples to comprehensive grain crystallization and development (Munir, Ahmed, Saqib, & Anis-ur-Rehman, 2016). Also, it has been reported in literature that the hindrance in the development grains of the ferrite is the presence of formed NdFeO_3 phase located near the grain boundary. It may also be suggested that the introduction of the Nd^{3+} ions cause lattice stresses and a chaotic lattice structure. These variations confine grain crystallization and delay the grain evolution, consequently reducing the crystallite dimensions (Peng et al., 2011).

3.2. Spectroscopic Analysis

Fourier transform infrared analysis deliver the data about the chemical changes and possession of the cations on different sites. Figure 4 shows the Fourier transform infrared analysis of $\text{Ni}_{0.4}\text{Co}_{0.6}\text{Nd}_x\text{Fe}_{2-x}\text{O}_4$ ferrites for $0.00 \leq x \leq 0.08$. In different compositions of prepared ferrites, in the range from 400 to 600 cm^{-1} two characteristics peaks were observed (Junaid et al., 2016). FTIR spectral analysis reveal the existence of characteristics bands that are ascribed to prepared nickel cobalt spinel ferrites. Commonly, the band with higher frequency located in 500 to 600 cm^{-1} range characterizes the fundamental vibration of tetrahedral group, whereas the lesser frequency band in the range of 400–500 cm^{-1} represents the octahedral groups. These bands are characteristic feature of spinel ferrites (Dasan et al., 2017).

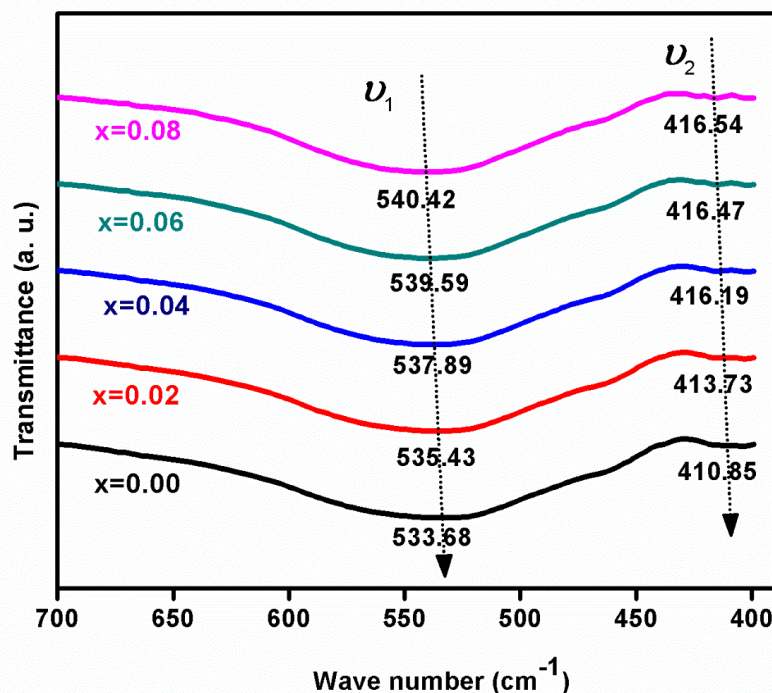


Figure 4: FTIR spectra of $\text{Ni}_{0.4}\text{Co}_{0.6}\text{Nd}_x\text{Fe}_{2-x}\text{O}_4$ with $0.00 \leq x \leq 0.08$

From the figure 4, it has observed that with the decrease in concentration of neodymium, the shifting of bands toward the lower wave number was noted. The bond length of octahedral site is greater than as compared to bond length of tetrahedral site causing the vibration of characteristics group seemed at smaller frequency in octahedral site than the tetrahedral site (Dasan et al., 2017).

Absorption at frequency around ν_2 (400-500 cm^{-1}) is produced by elongating of the octa-hedral oxygen and metallic bond, while the absorption at frequency around ν_1 (500-600 cm^{-1}) is caused by oxygen in the direction perpendicular to the axis joining the tetrahedral ion and oxygen (Shobana, Kwon, & Choe, 2012). Likewise, very intense peaks in range of 2900 cm^{-1} region can be attributed to C-H stretching frequencies. These were originated from the defect sites that exist within the structure of Nd doped Ni-Co ferrites. Supplementary, the bands displays absorption bands at 1396 cm^{-1} conforming to the presence of carboxyl group (COO^-). The band for carbon oxygen stretching is also present at 1244 cm^{-1} . There are also the bands with frequencies 1062 cm^{-1} and 890 cm^{-1} which show the presence of Fe-Co alloy system. The frequency band which present at 3672 cm^{-1}

¹ associated to oxygen-hydrogen vibration due to presence of absorbed water or moisture at surface. These observed peaks are tabulated in Table 2 (Rana, Philip, & Raj, 2010).

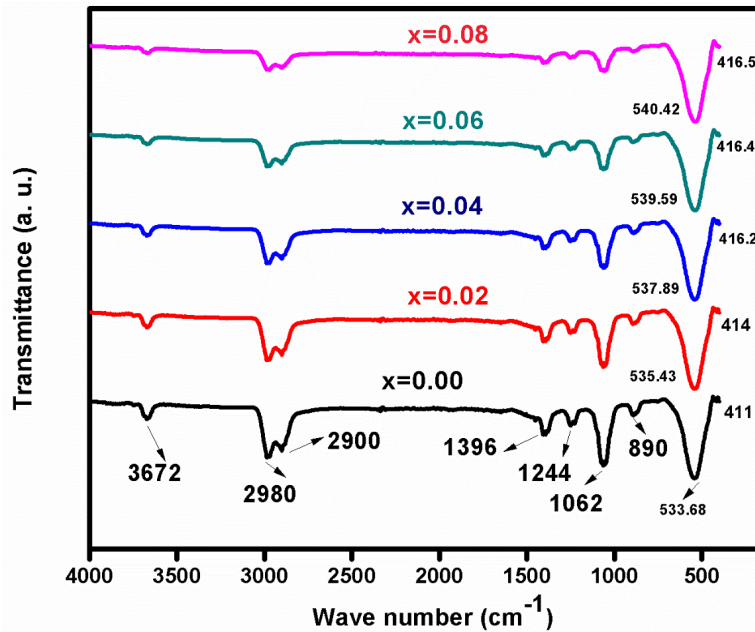


Figure 5: FTIR spectra of Ni_{0.4}Co_{0.6}Nd_xFe_{2-x}O₄ with 0.00 ≤ x ≤ 0.08

Table 2

FTIR spectral bands of annealed Ni_{0.4}Co_{0.6}Nd_xFe_{2-x}O₄ ferrites nanoparticles from figure 4 and 5

Samples' Composition	Frequency (cm ⁻¹)	Representations of Appeared Bands
Ni _{0.4} Co _{0.6} Nd _x Fe _{2-x} O ₄ ferrites	3672	(H-O) of free or absorbed water
(0.00 ≤ x ≤ 0.08)	2980, 2900	(C-H) stretching frequencies
Annealed at 950oC for 6 hours	1396	(COO-) carboxyl group
	1244	(C-O) stretching frequency
	1062, 890	Iron-Cobalt alloys
	540.42 to 533.68	Spinel characteristic (Fe-O) (tetrahedral)
	410.85 to 416.54	Spinel characteristic (Fe-O) (octahedral)

It has been revealed from the Fourier transform infrared analysis that the intensity of ν_2 rises with neodymium increasing concentration. The cause of this intensity variation is neodymium ion preference to go at B site and pushes the Fe ion to A site by increasing concentration of Nd and rises the radius of B-site (Dasan et al., 2017). The following formulae were used to found the force constants K_o and K_t :

$$K_o = 0.942128M \nu_2^2 / (M+32) \tag{4}$$

$$K_t = (2)^{1/2} K_o \nu_1 / \nu_2 \tag{5}$$

Here K_o is octahedral site force constant and K_t is tetrahedral site force constants. M represents molecular weight, ν_1 for frequency at tetrahedral and ν_2 frequency at octahedral site. From Table 3 it was observed that both K_o and K_t keep on increasing with increasing Nd³⁺ concentration.

$$R_{tetra} = a (3)^{1/2} (u - 0.25 - R_o) \tag{6}$$

$$R_{octa} = a (5/8 - u) - R_o \tag{7}$$

Where a represents lattice constant, u is oxygen positional parameter, R_o represents oxygen radius, tetrahedral radii is R_{tetra} and octahedral radii (1.32Å) is R_{octa} . For FCC crystal, the value of oxygen parameter is 0.375Å. Table 3 shows, it has been observed that the tetrahedral and octahedral radii decreased with the addition of Nd³⁺ contents and the bond length decreases with the rise of Nd concentration (Junaid et al., 2016).

Table 3

Molecular Weight, Characteristics frequencies, K_o , K_t , sample composition and Radii at octahedral and tetrahedra sites for $Ni_{0.4}Co_{0.6}Nd_xFe_{2-x}O_4$ ferrites ($0.00 \leq x \leq 0.08$)

Composition	Weight (gm/mole)	ν_1 (cm^{-1})	ν_2 (cm^{-1})	K_o (dyne/ cm^2) $\times 10^5$	K_t (dyne/ cm^2) $\times 10^5$	R_o	R_t
$Ni_{0.4}Co_{0.6}Fe_2O_4$	234.523	533.68	410.85	1.399353	1.817711	0.7733	0.24994
$Ni_{0.4}Co_{0.6}Nd_{0.02}Fe_{1.98}O_4$	236.291	535.43	413.73	1.420316	1.838107	0.7716	0.24869
$Ni_{0.4}Co_{0.6}Nd_{0.04}Fe_{1.96}O_4$	238.059	537.89	416.19	1.438531	1.859178	0.7682	0.24616
$Ni_{0.4}Co_{0.6}Nd_{0.06}Fe_{1.94}O_4$	239.827	539.59	416.47	1.441726	1.86794	0.7717	0.24877
$Ni_{0.4}Co_{0.6}Nd_{0.08}Fe_{1.92}O_4$	241.595	540.42	416.54	1.443455	1.872741	0.7688	0.24659

3.3. Magnetic Properties

The magnetic hysteresis loops are shown in the figure 6 for the $Ni_{0.4}Co_{0.6}Nd_xFe_{2-x}O_4$ with step size $x = 0.00, 0.02, 0.04, 0.06$ and 0.08 . The small part from ($H = -840$ Oe to 0 Oe) and ($M = 0$ emu/g to 32 emu/g) is also there in set in the magnetic hysteresis loops figure 6 to show change in values of M Vs H with change in concentration of doped neodymium. The small area of the hysteresis loops showed the magnetic behavior of the prepared ferrites as soft magnet. The energy dissipated during the setback of applied magnetic field responsible for the hysteresis loop area. Many aspects like porosity, density, grain size and chemical composition are also influencing the outline and size of the loops, that also affected by the sintering process, heat treatment conditions and preparation method etc. (Kadam, Shinde, Yadav, Patil, & Rajpure, 2013).

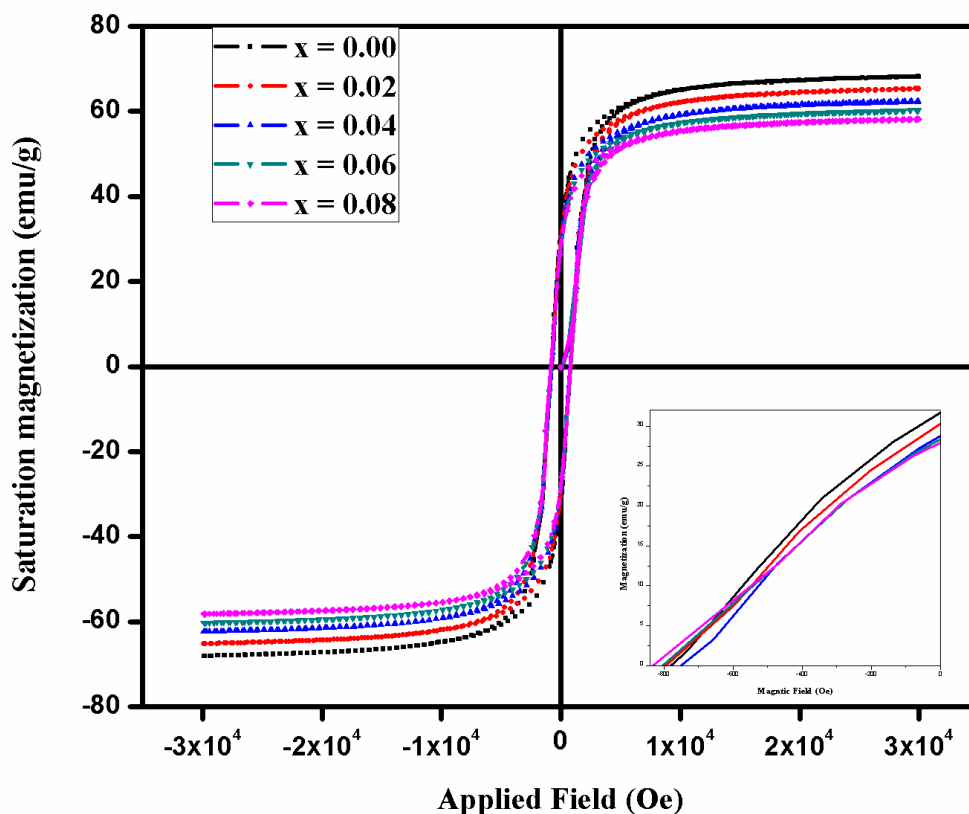


Figure 6: MH loops of $Ni_{0.4}Co_{0.6}Nd_xFe_{2-x}O_4$ with $0.00 \leq x \leq 0.08$

The measurements for parameters like H_c , M_s and (M_r) were calculated from loops in hysteresis MH curves and presented in the figure 7. It has been revealed from the figure 7 that the (M_s) values for undoped nickel cobalt ferrite base sample is greater with comparison of the Nd^{3+} ion replaced models because of high crystallinity (Dasan et al., 2017).

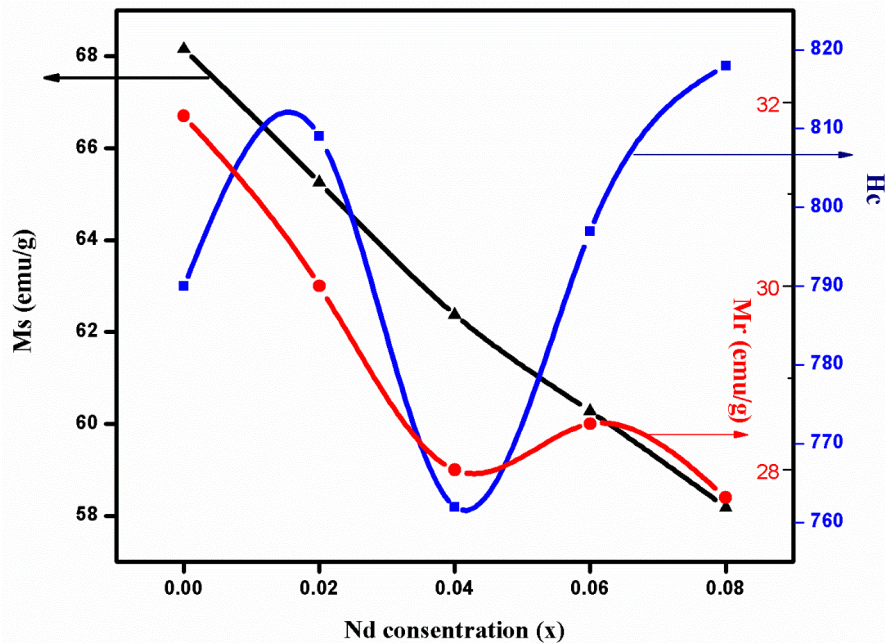


Figure 7: Saturation Magnetization (M_s) Vs Nd concentration of $\text{Ni}_{0.4}\text{Co}_{0.6}\text{Nd}_x\text{Fe}_{2-x}\text{O}_4$ with $0.00 \leq x \leq 0.08$

3.3.1. Saturation Magnetization (M_s)

It is clear from the figure 7 that M_s is decreasing with the increase in Nd^{3+} concentration. The reduction in M_s can be associated to the strong irreversible movement and movement of the domain wall in the applied magnetic field direction. The domain wall energy that hindering the displacement for occurring should be higher than the external applied field. Therefore, the tougher the displacement to occur will results in the reduction of the M_s . Further-more, magnetization may be defined as $M = |M_b - M_a|$, M decreases by the replacements at B-site (Peng et al., 2011). The replacing Nd^{3+} ions rather employed the B-site owing to their large ionic radii. The magnetic moment of Fe^{3+} ions has larger value as of Nd^{3+} ions (Przeniosło et al., 1996). This work results also show accordance with it as magnetic moment shows a decreasing trend with increasing Nd concentrations as prescribed in table 3. The decrease in the number of Fe^{3+} ions at B-site cause the decrease in magnetization at B-sublattice, showing the observed decrease in M_s with the Nd-substitution. The localized 4f electrons are the prime responsible factor for origin of the magnetic moments of rare earth metals which are considered by lower magnetic ordering temperatures. Thus, they exhibits disordered orientatins of their magnetic dipole moment at room temperature and later at room temperature they show paramagnetic behavior and contribute very slight to the magnetization of doped ferrite. With increase in neodymium contents, magnetization decreases at B-sub lattice. Moreover, Nd^{3+} ions addition by substitution of Fe^{3+} magnetic ions at B-site weakens A-B super exchange interactions. Therefore the ferrimagnetic ordering of nickel cobalt ferrite has been distressed due the substitution of Nd^{3+} ions and hence M_s decreases (Jacob, Thankachan, Xavier, & Mohammed, 2013).

3.3.2. Coercivity (H_c)

The overall trend of coercivity is increasing except for Nd concentration at $x = 0.04$ as compared with the H_c value of base sample having zero Nd concentration. It is observed that H_c first increase and then decrease from $x = 0.02$ to $x = 0.04$ and then increases for further doping from $x = 0.04$ to 0.08. This one step decrease in coercivity at $x = 0.04$ may be due to one of the any reason as H_c is depends upon microstructural property, further having dependence on presence of nonmagnetic atoms, strain and defects etc. present in the material, porosity and anisotropy in magneto crystalline. Also, this increasing trend of H_c except $x = 0.04$ is in reciprocal relation with decreasing saturation magnetization values by increasing the concentration of doped rare earth metal neodymium. The effect of induced strain is the increase due to additional doping to the deformation of the spinel

lattice and the surplus presence of Nd^{3+} ions in the lattice causes an increase in magneto crystalline anisotropy (Singhal, Barthwal, & Chandra, 2006).

Table 4

Saturation Magnetization, Retentivity, Coercivity, Remanence ratio and magnetic moment of $\text{Ni}_{0.4}\text{Co}_{0.6}\text{Nd}_x\text{Fe}_{2-x}\text{O}_4$ ($0.00 \leq x \leq 0.08$)

Composition	M_s (emu/gm)	M_r (emu/gm)	Remanence $R = M_r / M_s$	H_c (Oe)	Magnetic moment μ_B
$\text{Ni}_{0.4}\text{Co}_{0.6}\text{Fe}_2\text{O}_4$	68.16	31.85	0.467282864	790	2.86215
$\text{Ni}_{0.4}\text{Co}_{0.6}\text{Nd}_{0.02}\text{Fe}_{1.98}\text{O}_4$	65.26	30	0.459699663	809	2.761032
$\text{Ni}_{0.4}\text{Co}_{0.6}\text{Nd}_{0.04}\text{Fe}_{1.96}\text{O}_4$	62.38	28	0.448861815	765	2.658931
$\text{Ni}_{0.4}\text{Co}_{0.6}\text{Nd}_{0.06}\text{Fe}_{1.94}\text{O}_4$	60.28	28.5	0.47279363	797	2.588501
$\text{Ni}_{0.4}\text{Co}_{0.6}\text{Nd}_{0.08}\text{Fe}_{1.92}\text{O}_4$	58.19	27.8	0.477745317	818	2.517174

Another way to explain the coercivity is the grain size. There is inverse relation between coercivity and grain size. A higher number of domain walls are there for the larger grains. The less amount of energy needed for the magnetization or demagnetization by domain wall movement as compared to that of due to domain rotation. Opposite to this, With the increase in grain size, movement of walls increases with the higher number of grain walls and this influences magnetization or demagnetization caused by domain rotation (Costa, Tortella, Morelli, & Kiminami, 2003). Consequently, lower coercivity values are expected for the samples having larger grains and vice versa. This may be important reason in coercivity values for the synthesized nickel cobalt ferrites with doping of Nd^{3+} ions for $0.00 \leq x \leq 0.08$. Also, the presence of impurities which are distributed in the grain boundary are a pause and go counter to the domain walls displacement. Because of the presence of the secondary phase NdFeO_3 and the corresponding, the higher coercivity values are expected for samples with more Nd^{3+} ions as shown in Table 4 (Peng et al., 2011).

3.3.3. Remanence Ratio (R)

The "remanence ratio $R = M_r / M_s$ is a sign of the comfort by which the direction of magnetization reoriented to most nearly easy axis magnetization direction after the removal magnetic field". The isotropic nature of the synthesized samples is being revealed from the lower value of R (Shirsath, Toksha, & Jadhav, 2009). From Table 4, it can be observed that the variation in R with changing compositions is comparable to H_c . Therefore doping of Nd^{3+} in nickel-cobalt nanoferrite lead to the decrease in magnetic hysteresis loss for the nanocrystals. Also the sample $\text{Ni}_{0.4}\text{Co}_{0.6}\text{Nd}_{0.04}\text{Fe}_{1.96}\text{O}_4$ showed the minimum loss. The decrease in magneto crystalline anisotropy and grain growth because of doping of neodymium could be the major reason for the hysteresis loss reduction for doped ferrites from $x = 0.02$ to $x = 0.04$. The value of saturation magnetization is lower in comparison with undoped base sample of nickel-cobalt ferrites. It may be clarified by means of the core-shell model, which states that the effects due to finite size of the nanocrystals may lead to a canting of spins on the surface and thus decreases the magnetization (Jacob et al., 2013).

Conclusion

Sol-gel auto combustion method was used to synthesize the nickel cobalt nanoferrites with neodymium doping to study the structural, spectral and magnetic properties. The observed results are being discussed in this conclusion. The X-ray diffraction patterns of the prepared samples confirmed the spinel phases. An extra peak was observed for the samples with concentration of neodymium $x \geq 0.04$ that shows the formation of NdFeO_3 . Some trivial changes are observed in lattice constant and the crystallite size. Lattice constant found first to decrease up to $x = 0.04$ then increase for $x = 0.06$ and again decrease for $x = 0.08$. The reduction in the crystallite size as compared to base sample was observed by adding neodymium in nickel cobalt nanoferrites with slight increase after $x > 0.04$. The cubic spinel characteristics frequency bands were also there in FTIR spectra with shifting towards lower wave number with decrease in neodymium concentrations. Other peaks were also observed in FTIR spectra showing the presence of different stretching frequency vibrations for the samples. Tetrahedral and octahedral radius were calculated. Force constants showed the decreasing behavior with the increase in

neodymium concentration. A decreasing trend was observed for the saturation magnetization with increase in neodymium doping as compared to undoped nickel cobalt ferrites. The coercivity value was also found in increasing order as compared to base sample except $x = 0.04$. The variation in remanence ratio was similar to that of coercivity.

References

- Anis-ur-Rehman, M., Ansari, M., Mughal, Z. U. N., Awan, M., & Maqsood, A. (2012). *Synthesis and Thermoelectric Studies in Cr Doped Cobalt Ferrites Nano Particles*. Paper presented at the Key Engineering Materials.
- Anupama, M., & Rudraswamy, B. (2016). *Effect of Gd³⁺-Cr³⁺ ion substitution on the structural, electrical and magnetic properties of Ni-Zn ferrite nanoparticles*. Paper presented at the IOP Conference Series: Materials Science and Engineering.
- Cannas, C., Falqui, A., Musinu, A., Peddis, D., & Piccaluga, G. (2006). CoFe₂O₄ nanocrystalline powders prepared by citrate-gel methods: synthesis, structure and magnetic properties. *Journal of Nanoparticle Research*, 8(2), 255-267.
- Costa, A., Tortella, E., Morelli, M., & Kiminami, R. (2003). Synthesis, microstructure and magnetic properties of Ni-Zn ferrites. *Journal of Magnetism and Magnetic Materials*, 256(1), 174-182.
- Dasan, Y., Guan, B., Zahari, M., & Chuan, L. (2017). Influence of La³⁺ Substitution on Structure, Morphology and Magnetic Properties of Nanocrystalline Ni-Zn Ferrite. *PLoS one*, 12(1), e0170075.
- Farid, M., Ahmad, I., Aman, S., Kanwal, M., Murtaza, G., Ali, I., & Ishfaq, M. (2015). Structural, electrical and dielectric behavior of Ni_xCo_{1-x}Nd_yFe_{2-y}O₄ nano-ferrites synthesized by sol-gel method. *Digest Journal of Nanomaterials and Biostructures*, 10(1), 265-275.
- Farid, M. T., Ahmad, I., Murtaza, G., Ali, I., & Ahmad, I. (2016). Structural, Electrical and Dielectric Behavior of Ni_xCo_{1-x}PryFe_{2-y}O₄ Nano-Ferrites Synthesized by Sol-Gel Method. *Journal of the Chemical Society of Pakistan*, 38(6), 1064-1064.
- Hankare, P., Sankpal, U., Patil, R., Lokhande, P., & Sasikala, R. (2011). Synthesis, characterization and catalytic activity of chromium substituted cobalt ferros spinels. *Materials Science and Engineering: B*, 176(2), 103-109.
- Iqbal, M. J., & Siddiquah, M. R. (2008). Electrical and magnetic properties of chromium-substituted cobalt ferrite nanomaterials. *Journal of Alloys and Compounds*, 453(1), 513-518.
- Jacob, B. P., Thankachan, S., Xavier, S., & Mohammed, E. (2013). Effect of Tb³⁺ substitution on structural, electrical and magnetic properties of sol-gel synthesized nanocrystalline nickel ferrite. *Journal of Alloys and Compounds*, 578, 314-319.
- Junaid, M., Khan, M. A., Iqbal, F., Murtaza, G., Akhtar, M. N., Ahmad, M., . . . Warsi, M. F. (2016). Structural, spectral, dielectric and magnetic properties of Tb-Dy doped Li-Ni nano-ferrites synthesized via micro-emulsion route. *Journal of Magnetism and Magnetic Materials*, 419, 338-344.
- Kadam, A., Shinde, S., Yadav, S., Patil, P., & Rajpure, K. (2013). Structural, morphological, electrical and magnetic properties of Dy doped Ni-Co substitutional spinel ferrite. *Journal of Magnetism and Magnetic Materials*, 329, 59-64.
- Kriehle, K., Lo, C., Melikhov, Y., & Snyder, J. E. (2006). Investigation of Cr substitution in Co ferrite (CoCr_xFe_{2-x}O₄) using Mossbauer spectroscopy. *Journal of Applied Physics*, 99(8), 08M912.
- KULKARNI, V., BHUJBAL, M., & RATHOD, S. (2016). Influence of La³⁺ Doped Ni-Co Nanoferrite and Magnetic Properties by Sol-Gel Auto Combustion Method.
- Munir, A., Ahmed, F., Saqib, M., & Anis-ur-Rehman, M. (2016). Partial correlation of electrical and magnetic properties of Nd substituted Ni-Zn nanoferrites. *Journal of Magnetism and Magnetic Materials*, 397, 188-197.
- Pardavi-Horvath, M. (2000). Microwave applications of soft ferrites. *Journal of Magnetism and Magnetic Materials*, 215, 171-183. doi:10.1016/S0304-8853(00)00106-2
- Peng, Z., Fu, X., Ge, H., Fu, Z., Wang, C., Qi, L., & Miao, H. (2011). Effect of Pr³⁺ doping on magnetic and dielectric properties of Ni-Zn ferrites by "one-step synthesis". *Journal of Magnetism and Magnetic Materials*, 323(20), 2513-2518.
- Przeniosło, R., Sosnowska, I., Fischer, P., Marti, W., Bartolomé, F., Bartolomé, J., . . . Sonntag, R. (1996). Magnetic moment ordering of Nd³⁺ and Fe³⁺ in NdFeO₃ at low temperature. *Journal of Magnetism and Magnetic Materials*, 160, 370-371.

- Rana, S., Philip, J., & Raj, B. (2010). Micelle based synthesis of cobalt ferrite nanoparticles and its characterization using Fourier Transform Infrared Transmission Spectrometry and Thermogravimetry. *Materials Chemistry and Physics*, 124(1), 264-269.
- Shirsath, S. E., Toksha, B., & Jadhav, K. (2009). Structural and magnetic properties of In³⁺ substituted NiFe₂O₄. *Materials Chemistry and Physics*, 117(1), 163-168.
- Shobana, M., Kwon, H., & Choe, H. (2012). Structural studies on the yttrium-doped cobalt ferrite powders synthesized by sol-gel combustion method. *Journal of Magnetism and Magnetic Materials*, 324(14), 2245-2248.
- Singhal, S., Barthwal, S., & Chandra, K. (2006). XRD, magnetic and Mössbauer spectral studies of nano size aluminum substituted cobalt ferrites (CoAl_xFe_{2-x}O₄). *Journal of Magnetism and Magnetic Materials*, 306(2), 233-240.